EasyChair Preprint

№ 8977

A Unified Control Framework for Grid-Forming Inverters

Armando José Gomes Abrantes Ferreira,
Alexandre Cunha Oliveira and Antonio Marcus Nogueira Lima

October 3, 2022

A Unified Control Framework for Grid-Forming Inverters ⋆

Armando J.G. Abrantes-Ferreira, Alexandre C. Oliveira, Antonio M.N. Lima *

* *Graduate Program in Electrical Engineering (PPgEE), Universidade Federal de Campina Grande (UFCG), PB (e-mail: armando.ferreira@ee.ufcg.edu.br, {aco,amnlima}@dee.ufcg.edu.br).*

Abstract: Two Grid-Forming (GFM) control strategies based on emulation of Synchronous Machine (SM) behavior, namely Droop Control and Synchronverter, and two Andronov-Hopf Dispatchable Virtual Oscillator Control (dVOC)-based techniques are unified into a compact yet generalized control framework for GFM inverters. In the light of the proposed framework, we reassess the control laws of the studied GFM analytically, and further validate these analyzes *in silico* for steady-state power sharing and transient responses. We show how the mathematical structures of the studied GFM methods differ and resemble, which has an impact on the underlying grid forming performance. These differences are attributed to intrinsic nonlinearities, which can be translated as operating point parameter dependence for each GFM technique being recast for the suggested framework. Furthermore, we show that, to a certain extent, the techniques can be parameterized to have similar steady-state and dynamic responses. This work succeed in developing a technology-agnostic metrics for steady-state power sharing and dynamic behaviors of GFM methods, an important requisite for the interoperability of grid-connected inverter units.

Keywords: Grid-Forming Control, Droop Control, Synchronverter, Virtual Oscillator Control

1. INTRODUCTION

The increasing demand for electrical energy in the last decades and the challenging goals on the reduction of greenhouse gas emissions are bringing many efforts to improve the Electrical Systems. The increasing penetration of alternative sources of energy (solar, wind, biomass, fuel cells) creates a sustainable environment for the establishment of Distributed Generation (DG), where system generation is also carried out by an increased number of dispersed generation units. Those units are located close to the consumer, which reduces transmission losses, the demand for expansion and the re-powering of transmission lines, in addition to improvements in the voltage profile and increased reliability of the electrical system. Further discussions can be found in Matevosyan et al. (2021); Smith and Lew (2021).

Nevertheless, electrical grids operating with an advanced penetration of DG brings a much higher degree of complexity with regard to the control and coordination of a large number of generating units, taking into account that the current electrical systems still have a good part of their philosophy of operation and protection based on concentrated generation, as detailed in Milano et al. (2018). Therefore, in addition to opportunities, challenges arise for the growth in the number of DG units (Lin et al. (2022)).

On one hand, conventional power inverter control strategies have been based on the so-called grid-following (GFL) approach, with the inverter working as a controlled current source, as reviewed in Rosso et al. (2021). In these methods the grid frequency is estimated so that the injected current is regulated to track pre-defined power set points, as further explained by Bouzid et al. (2015). However, these strategies do not provide damping to grid stability so, as the penetration of DG increases, it becomes clear that extra damping have to be provided to the future grid with reduced inertia. This latter topic was addressed insightfully in Lasseter et al. (2019).

GFM strategies, on the other hand, were developed initially aiming for compatibility between GFM inverters and current SM-based power systems. These methods emulate the characteristics of SM at different levels of abstraction. This class of GFM strategies include Droop Control (Meng et al. (2018)), Power Synchronization Control (Wu and Wang (2018)), Synchronverter (Gomes et al. (2022)), Virtual Synchronous Machine (VSM/VISMA) (Ebrahimi et al. (2019)) and Matching Control(Arghir and Dörfler (2019)). These techniques have been widely investigated in recent years, taking advantage of their simple and intuitive implementations and their backward compatibility with legacy power systems. However, there are some inconsistencies in matching the models of converters and synchronous machines, as addressed by Alassi et al. (2020).

Another class of promising approaches for controlling GFM inverters is the so-called Virtual Oscillator Control (VOC) methods, inspired by the phenomenon of synchronization in networks of coupled oscillators. These methods offer almost global synchronization and embeds droop control law close to steady-state (Tôrres et al. (2015);

⋆ The authors thank PPgEE/UFCG for funding this work. This study was financed in part by Coordenação de Aperfeiçoamento de Pessoal de Nível Superior - Brasil (CAPES) Finance Code 001.

Johnson et al. (2013)). However, these techniques are not dispatchable, which makes them unsuitable for grid-connected operation. Recently, dispatchable VOC (dVOC) techniques were proposed in Colombino et al. (2019); Lu et al. (2019). However, the steady-state droop relationships of these techniques are highly nonlinear, which may bring extra computational burden for the challenging task in seeking for optimal droop coefficients/power set points in secondary/tertiary control layers (Baker et al. (2017)). A dVOC-based technique was recently proposed in Abrantes-Ferreira and Lima (2021), where the technique has shown similar dynamic response compared to the technique presented in Lu et al. (2019) whereas it presented linear droop behavior for purely resistive or inductive lines.

The interoperability of grid-connected inverter units controlled by different strategies may be challenging, as there is a variety of techniques without a unified guideline with common performance metrics, as highlighted by O'Malley et al. (2021). Some previous works have attempted to unify GFM controllers such as in D'Arco and Suul (2013); Sinha et al. (2015), but these works focused in comparative analyzes of pairs of GFM methods. Recently Johnson et al. (2022) presented a first attempt of a unified control framework for GFM controllers, analyzing the similarities in the structure of three GFM techniques. However, the similarities between the GFM techniques outlined by this framework are only morphological, i.e., the corresponding parameters of each GFM technique do not have a common physical meaning.

The main contribution of this work is to develop a unified GFM control framework which consolidates important existing GFM strategies into an generalized control model, defining technology-agnostic metrics for steady-state and dynamic behaviors of GFM methods. We show that applying algebraic manipulation on the control laws of the studied GFM techniques allows us to reassess them in such a way that they all acquire a similar structure, with internal model voltage, frequency and phase as states. We show that, to a certain extent, the techniques can be parameterized to have similar steady-state and dynamic responses. To validate the proposed framework, we compare the techniques based on simulations confirming the predicted similarities and differences between their operations.

The remaining of this work is organized as follows: Section 2 addresses the discussion of three popular GFM strategies, introducing the control law, steady-state droop relationships and tuning criteria for each method. In Section 3 we propose a unified framework for GFM inverters, discussing its control law and how one can reconstruct each studied GFM with proper configuration of the proposed model. In Section 4 we compare the GFM methods based on simulations concerning steady state droop relationships and dynamics of voltage and frequency. Conclusions are drawn in Section 5.

2. GFM METHODS

In regard to the GFM strategies aforementioned, in this section four different GFM methods are discussed, starting with Droop Control, as the baseline solution for the operation of GFM inverters, then with Synchronverter and finish with two Andronov-Hopf Dispatchable Virtual Oscillator Control (AH-dVOC) methods.

Consider the system depicted in Figure 1, which represents a voltage source converter (VSC) system connected to a constant impedance linear load. We consider this is the best system to characterize the actuation of the GFM techniques, since the role of generator and load for each unit is well defined in this setup. Furthermore, the dynamics of voltage and frequency will be determined by the inverter actuation. The inverter is controlled by a GFM strategy, which receives the signals of voltage and current measured at the output of the VSC system and defines the voltage reference vector $\mathbf{v}$. Taking the average over a switching period, the VSC system can be regarded as a unity gain block, so that $\mathbf{e} \approx \mathbf{v}$. The output voltage of the inverter represented in Figure 1 frame is defined in the stationary $\alpha\beta$-reference as $\mathbf{v}_{g\alpha\beta} = v_{g\alpha} + jv_{g\beta}$.

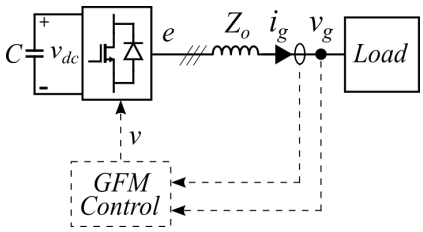

Figure 1. Simplified VSC System Connected to a Constant Impedance Loadq.

In this work, for a balanced three-phase set $\mathbf{x}_{\text{abc}} = [x_a \;\; x_b \;\; x_c]^T$, its representation in the stationary $\alpha\beta$-reference frame is carried out by means of Clarke transformation, which is consistently explored by O'Rourke et al. (2019). Throughout this work it is assumed that amplitude-invariant Clarke transformation is applied. The resulting space vector is described by

$$\mathbf{x}_{\alpha\beta} = \underbrace{X\sin(\theta)}_{x_\alpha} + j\underbrace{[-X\cos(\theta)]}_{x_\beta}, \tag{1}$$

where X and $\theta = \arctan(x_\beta/x_\alpha)$ stand for the amplitude and phase angle of $\mathbf{x}_{\alpha\beta}$, respectively, and $j = \sqrt{-1}$ represents the imaginary unit.

2.1 Droop Control

Sun et al. (2017) highlights that droop control can be considered the baseline solution to GFM control, since it is based on the behavior of the conventional speed droop control of synchronous machines, where the deviations in the imposed voltage and frequency are proportional to the deviations between the supplied and reference active and reactive powers, similar to speed control by Droop curves of synchronous generators.

For grids with characteristics dominantly inductive, the droop relationships can be expressed by (2) and (3):

$$\begin{aligned} E &= V^* + m_p\Delta\bar{p}, \\ \omega &= \omega^* + m_q\Delta\bar{q}, \end{aligned} \tag{2}$$

$$\begin{aligned} \frac{1}{\omega_p}\frac{d}{dt}\Delta\bar{p} &= -\Delta\bar{p} + (p^* - p), \\ \frac{1}{\omega_q}\frac{d}{dt}\Delta\bar{q} &= -\Delta\bar{q} + (q^* - q), \end{aligned} \tag{3}$$

where ω^* and V^* stand for the references of frequency and voltage, respectively; m_p and m_q are P/f and Q/V droop coefficients, respectively; $\Delta\bar{p}$, $\Delta\bar{q}$, p, q, p^* and q^* are filtered active and reactive power deviations, measured active and reactive power and references for active and reactive power, respectively; ω_p and ω_q are the cutoff frequencies of the LPFs for active and reactive powers, respectively.

The internal voltage reference vector $e_{\alpha\beta}$ is provided to outer control loops for multi-loop droop control or to PWM modulator for single-loop droop control. The implication of applying single-loop or multi-loop philosophies in droop control is explored in Du et al. (2019), where the authors find distinctive characteristics for dynamic performance and stability boundaries for each approach.

Isolating $\Delta\bar{p}$ and $\Delta\bar{q}$ in (2) and substituting in (3) we can describe control law for regulation of E and ω

$$\begin{aligned}\left(\frac{1}{\omega_q}\right)\frac{d}{dt}E &= (V^* - E) + m_q(q^* - q),\\ \left(\frac{1}{\omega_p}\right)\frac{d}{dt}\omega &= (\omega^* - \omega) + m_p(p^* - p).\end{aligned} \tag{4}$$

For steady state condition we set the time derivates to zero, obtaining the relationship

$$\begin{aligned}E &= V^* + m_q(q^* - q),\\ \omega &= \omega^* + m_p(p^* - p).\end{aligned} \tag{5}$$

The tuning criteria for gains m_p and m_q is based on steady power sharing specifications and can be formularized by setting the time derivatives and the references of active and reactive powers in (17) to zero, yielding to

$$m_p = \frac{\Delta\omega_{\max}}{P_R}, \quad m_q \quad = \frac{\Delta V_{\max}}{Q_R}, \tag{6}$$

where P_R and Q_R stand for rated active and reactive power, respectively. Maximum allowed deviations for frequency $\Delta\omega_{\max}$ and internal voltage $\Delta V_{\max}$ are given by

$$\Delta\omega_{\max} = d_\omega^{pu}\omega^*, \quad \Delta V_{\max} \quad = d_v^{pu}V^*, \tag{7}$$

where d_ω^{pu} and d_v^{pu} are the specified per-unit droop deviations of frequency and voltage, respectively.

2.2 Synchronverter Control

Synchronverter (Synch-VSM) model is obtained from the synchronous generator model that can be derived from the generalized symmetrical AC machine model with generator convention Leonhard (2001) in space vector representation. In this model, its virtual rotor current i_f is an adjustable parameter which makes this model having rotor dynamics similar to Permanent Magnet Synchronous Machine (PMSM) with adjustable flux. The model is further developed in the stationary $\alpha\beta$-reference frame by Gomes et al. (2022).

The virtual shaft of the synchronverter model can be represented as follows

$$\begin{aligned}K\frac{d}{dt}\psi &= (q^* - q) + D_q(V_g^* - V_g)\\ J\frac{d}{dt}\omega &= T_m - T_e + D_p(\omega^* - \omega),\end{aligned} \tag{8}$$

where J is the inertia coefficient, ω and ω^* are the actual and reference rotor angular speed, respectively. T_m and T_e are respectively the virtual mechanical and electrical torques. θ and D_p are the virtual rotor angle and frequency droop coefficient, respectively. ψ stands for the virtual flux, which regarding the model of synchronous machines define the Synchronverter model voltage E as

$$E = \psi\omega. \tag{9}$$

Virtual mechanical and electrical torques are given by

$$\begin{aligned}T_m &= \frac{p^*}{\omega^*},\\ T_e &= \frac{p}{\omega}.\end{aligned} \tag{10}$$

Applying amplitude invariant Clarke transformation instantaneous active and reactive powers as seen from the converter legs are defined as

$$\begin{aligned}p &= e_\alpha i_\alpha + e_\beta i_\beta,\\ q &= e_\beta i_\alpha - e_\alpha i_\beta,\end{aligned} \tag{11}$$

with

$$\mathbf{e} = \underbrace{\omega\psi\sin(\theta)}_{e_\alpha} + j\underbrace{\left[-\omega\psi\cos(\theta)\right]}_{e_\beta}. \tag{12}$$

Evaluation of the electrical torque equation yields:

$$T_e = \frac{e_\alpha i_\alpha}{\omega} + \frac{e_\beta i_\beta}{\omega}. \tag{13}$$

Substituting, we can rewrite the active power loop as

$$J\frac{d}{dt}\omega = \left(\frac{p^*}{\omega^*} - \frac{p}{\omega}\right) + D_p(\omega^* - \omega). \tag{14}$$

The dynamics of the internal voltage amplitude can be obtained by differentiating (9)

$$\frac{d}{dt}E = \frac{d}{dt}(\psi\omega) = \omega\frac{d}{dt}\psi + \psi\frac{d}{dt}\omega. \tag{15}$$

Substituting (8) into (15) as well as substituting (10) in second equation of (8) and manipulating, we can derive the expressions for the dynamics of Synchronverter model voltage and frequency of Synchronverter Control:

$$\begin{aligned}\left(\frac{K}{D_q}\frac{1}{\omega}\right)\frac{d}{dt}E &= (V_g^* - V_g) + \left(\frac{1}{D_q}\right)(q^* - q) +\\ &\left[\frac{KD_p}{JD_q}\frac{E}{\omega^2}\left(1 + \frac{1}{D_p}\frac{(\omega p^* - p\omega^*)}{\omega^*\omega(\omega^* - \omega)}\right)\right](\omega^* - \omega),\\ \left(\frac{J}{D_p}\right)\frac{d}{dt}\omega &= (\omega^* - \omega) +\\ &\left[\frac{1}{D_p}\frac{1}{\omega}\left(1 - \frac{(\omega^* - \omega)}{\omega^*}\frac{p^*}{(p^* - p)}\right)\right](p^* - p).\end{aligned} \tag{16}$$

The apparent singularity points seemingly taking place at $\omega = \omega^*$ and $p = p^*$ in the terms between brackets in (16) are cancelled out by the multiplication of the terms by the error of frequency and active power, respectively.

For steady state condition we set the time derivatives in second equation of (8) and (14), therefore we can establish (17)

$$\begin{aligned}V_g &= V_g^* + \frac{1}{D_q}(q^* - q),\\ \omega &= \omega^* + \frac{1}{D_p}\left(\frac{p^*}{\omega^*} - \frac{p}{\omega}\right).\end{aligned} \tag{17}$$

The tuning procedure for D_p is carried out considering that during operation in grid-connected mode the deviations of

frequency are small (Gomes et al. (2022)). Therefore, we consider $\omega \approx \omega^*$ in the second equation of (17), so that the frequency droop relationship can be obtained by (18)

$$\omega \approx \omega^* + \frac{1}{D_p \omega^*}(p^* - p), \tag{18}$$

with frequency droop coefficient given by

$$D_p \approx \frac{P_R}{\omega^* \Delta\omega_{\max}}, \tag{19}$$

with $\Delta\omega_{\max}$ given by (7).

Voltage droop coefficient can be defined as

$$D_q = \frac{Q_R}{\Delta V_{\max}}, \tag{20}$$

with $\Delta V_{\max}$ given by (7).

2.3 Nonlinear Droop Andronov-Hopf Dispatchable Virtual Oscillator Control (NLD-AH-dVOC)

A dVOC-based method was proposed in Lu et al. (2019), which works monitoring the inverter's output current $i_{\alpha\beta}$ and regulates the inverter's legs voltage by controlling the internal model voltage vector $\mathbf{e}_{\alpha\beta} = Ee^{j\omega t} = e_\alpha + je_\beta$, following the control law (21):

$$\frac{d}{dt}\mathbf{e}_{\alpha\beta} = (j\mathbf{e}_{\alpha\beta})\omega^* + \mu[(E^*)^2 - E^2]\mathbf{e}_{\alpha\beta} + \eta e^{j\phi}(\mathbf{i}^*_{\alpha\beta} - \mathbf{i}_{\alpha\beta}), \tag{21}$$

where the values μ, $\eta > 0$ are design parameters. $0 \leq \phi \leq \pi/2$ is a design parameter which is related to the line X/R characteristics, where $\phi = 0$ corresponds to purely resistive lines and $\phi = \pi/2$ to purely inductive lines. In this work we will consider $\phi = \pi/2$. E^* is the internal model voltage amplitude reference and $\mathbf{i}^*_{\alpha\beta}$ is the current amplitude reference.

From Akagi et al. (2017) the current reference vector can be obtained by

$$\mathbf{i}_{\alpha\beta}{}^* = \frac{2}{3}\frac{1}{E^2}(p^* - jq^*)\mathbf{e}_{\alpha\beta}, \tag{22}$$

The voltage amplitude E and phase angle θ are expressed by

$$E = \sqrt{e_\alpha^2 + e_\beta^2}, \quad \theta = \arctan\left(\frac{e_\beta}{e_\alpha}\right). \tag{23}$$

Differentiating (23) and substituting (21) and (22) we can obtain the expressions for the dynamics E and ω

$$\begin{aligned} \frac{d}{dt}E &= \mu E\Big[(E^*)^2 - E^2\Big] + \frac{2\eta}{3E}(q^* - q), \\ 0 &= (\omega^* - \omega) + \frac{2\eta}{3E^2}(p^* - p). \end{aligned} \tag{24}$$

The expression of internal model voltage dynamics can be rewritten as

$$\left(\frac{1}{\mu}\frac{1}{E(E^* + E)}\right)\frac{d}{dt}E = (E^* - E) + \left(\frac{2\eta}{3\mu}\frac{1}{E^2(E^* + E)}\right)(q^* - q). \tag{25}$$

Setting the time derivative of E in (24) to zero and, simplifying, the expressions for voltage and frequency in steady-state can be obtained as:

$$\begin{aligned} E^2 &= (E^*)^2 + \frac{2\eta}{3\mu E^2}(q^* - q), \\ \omega &= \omega^* + \frac{2\eta}{3E^2}(p^* - p), \end{aligned} \tag{26}$$

which reveal a nonlinear coupled P/f, Q/V droop behavior.

The analytic expression for E can be obtained as (27):

$$E = \sqrt{\frac{1}{2}\left((E^*)^2 + \sqrt{(E^*)^4 + \frac{8\eta}{3\mu}(q^* - q)}\right)} \tag{27}$$

The procedure presented here to determine parameters μ and η is inspired by the approach presented by Awal and Husain (2020). We set $p^* = 0$ in (26) and consider that with operation at rated active and reactive powers E and ω are at their minimum allowable values. The following expressions can be derived

$$\begin{aligned} \eta &= \frac{3}{2}\frac{\Delta\omega_{\max}}{P_R}E^2_{\min}, \\ \mu &= \frac{2\eta}{3}\frac{Q_R}{E^2_{\min}[(E^*)^2 - E^2_{\min}]}, \end{aligned} \tag{28}$$

with $\Delta\omega_{\max}$ given by (7) and minimum allowed voltage $E_{\min}$ given by

$$E_{\min} = (1 - d_v^{pu})E^*. \tag{29}$$

2.4 Linear-Droop AH-dVOC (LD-AH-dVOC)

A different AH-dVOC-based GFM strategy was proposed by Abrantes-Ferreira and Lima (2021), bringing enhancements to the family of dVOC-based techniques concerning its linear decoupled droop behavior for purely inductive or resistive lines.

In this strategy, the internal model voltage vector is controlled following the control law:

$$\frac{d}{dt}\mathbf{v}_{\alpha\beta} = j\omega_o\mathbf{v}_{\alpha\beta} + \sigma(\|\mathbf{v}^*_{\alpha\beta}\| - \|\mathbf{v}_{\alpha\beta}\|)\mathbf{v}_{\alpha\beta} + \rho e^{j\phi}\|\mathbf{v}_{\alpha\beta}\|^2(\mathbf{i}^*_{\alpha\beta} - \mathbf{i}_{\alpha\beta}), \tag{30}$$

where the values $\sigma, \rho > 0$ are design parameters. Parameters ϕ, E^* and $i^*_{\alpha\beta}$ are similar to those defined in Section 2.3. In this work, we also consider $\phi = \pi/2$ for LD-AH-dVOC.

Using the same approach as was employed in Section 2.3, one can obtain the expressions for the dynamics of E and ω as expressed in (31):

$$\begin{aligned} \frac{d}{dt}E &= E\Big[\sigma(E^* - E) + \frac{2\rho}{3}(q^* - q)\Big], \\ 0 &= (\omega^* - \omega) + \frac{2\rho}{3}(p^* - p). \end{aligned} \tag{31}$$

The expression of internal model voltage dynamics can be rewritten as

$$\left(\frac{1}{\sigma}\frac{1}{E}\right)\frac{d}{dt}E = (E^* - E) + \frac{2\rho}{3\sigma}(q^* - q). \tag{32}$$

Similarly, we set the time derivative of E in (31) to zero and, simplifying, the droop expressions for voltage and frequency for inductive lines in steady-state can be obtained as:

$$\begin{aligned} E &= E^* + \frac{2\rho}{3\sigma}(q^* - q), \\ \omega &= \omega^* + \frac{2\rho}{3}(p^* - p), \end{aligned} \tag{33}$$

which disclose a steady state coupling-free linear P/f, Q/V droop behavior, similar to Conventional Droop Control.

The tuning criteria for gains ρ and σ is also based on steady power sharing specifications, where we set the references of active and reactive powers in (33) to zero, yielding to

$$\begin{aligned} \rho &= \frac{3}{2}\frac{\Delta\omega_{\max}}{P_R}, \\ \sigma &= \frac{2\rho}{3}\frac{Q_R}{\Delta E_{\max}}. \end{aligned} \tag{34}$$

Maximum allowed deviation of internal model voltage $\Delta E_{\max}$ is given by (35)

$$\Delta E_{\max} = d_v^{pu} E^*. \tag{35}$$

3. UNIFIED GFM CONTROL FRAMEWORK

The GFM methods studied in the Section 2 are now defined in a generalized approach, observing similarities in their structure. We propose in this work the studied GFM control methods to be seen as instantiations of our proposed unified GFM control framework.

The proposed unified GFM control framework is described by (36):

$$\begin{aligned} \tau_v \frac{d}{dt}E &= (E^* - E) + K_q(q^* - q) + K_{vf}(\omega^* - \omega), \\ \tau_f \frac{d}{dt}\omega &= (\omega^* - \omega) + K_p(p^* - p), \end{aligned} \tag{36}$$

where $\tau_v(\omega, E)$ and $\tau_f(\omega, E)$ are the voltage and frequency-dependent *time constants* for the internal voltage and frequency states, respectively. $K_q(\omega, E)$, $K_p(p, \omega, E)$ are the active and reactive droop coefficients, respectively. $K_{vf}(p, \omega, E)$ is the coefficient accounting for coupling between active and reactive power loops. In this text, (ω, E) and (p, ω, E) were dropped from all active power, voltage and frequency-dependent parameters for the sake of optimizing space *usus*.

The block diagram of proposed GFM control framework is shown in Figure 2. Its configuration for each studied GFM Method is shown in Table 1.

3.1 Some Insights on the Studied GFM Methods

We now have a discussion about each GFM technique in light of the proposed framework, characterizing the methods considering the behavior of the parameters that govern their steady-state and dynamic operations.

From the first line of Table 1, it can be seen that Droop control has an important characteristic of constant parameters, which reveal that the steady-state and dynamic behaviors of this control technique does not change according to the operating point. Moreover, we can see that the time constants of voltage and frequency are tunable and determined solely by the cutoff frequencies ω_p and ω_q.

The voltage which is considered for regulation in Droop Control is the voltage at the output of the inverter, i.e., V_g in Figure 1. Furthermore, the voltage which is used to calculate active and reactive powers is the voltage at the output of the inverter.

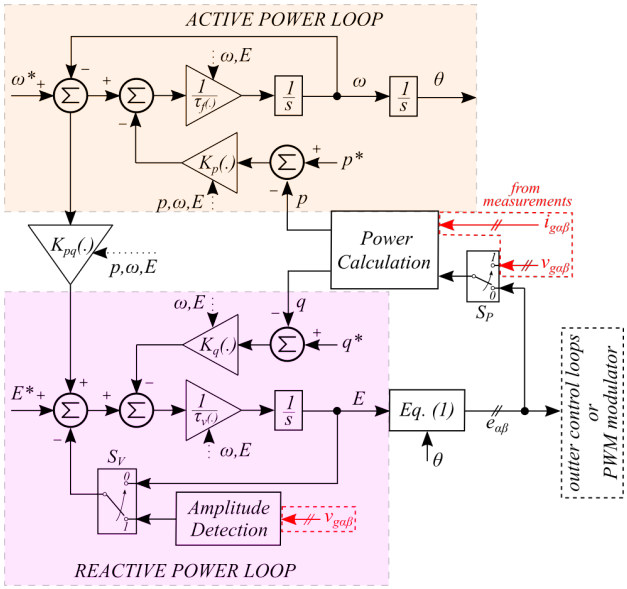

Figure 2. Block Diagram of Proposed Generalized GFM Framework Control, with parameterization defined in Table 1.

Synchronverter, another SM-inspired technique, has its parameterization given in the second line of Table 1. We can see that the parameters K_q, which governs the steady-state power sharing of reactive power, and τ_f, the tunable time constant of frequency are constant. On the other hand, the parameters K_p, which governs the steady-state power sharing of active power, and τ_v, the tunable time constant of voltage, are dependent of the operating point of the inverter, which may bring extra undesirable nonlinearities for the operation of the inverter.

The term K_{vf}, which accounts for a coupling between active and reactive power loops, appears exclusively in the expression for dynamics of voltage of the Synchronverter model. From (16):

$$K_{vf}^S(p, \omega, E) = \frac{KD_p}{JD_q}\frac{E}{\omega^2}\left(1 + \frac{1}{D_p}\frac{(\omega p^* - p\omega^*)}{\omega^*\omega(\omega^* - \omega)}\right). \tag{37}$$

At steady state, however, this term vanishes as substituting the frequency value given by the second equation of (17) in (37).

In Synchronverter, the voltage which is considered for regulation is also V_g. However, the voltage which is used to calculate active and reactive powers is the voltage of the internal model of the control model. We believe the implication of this arrangement deserves further investigation.

From the third line of Table 1, we can see that all the parameters of NLD-AH-dVOC technique are dependent on internal voltage amplitude E, so that the operating points affects the steady-state power sharing and dynamic behaviors. Furthermore, as the time constant of the dynamics of voltage amplitude is a function of E, E^* and μ. we point out that this strategy does not allow specifying both steady-state power sharing and voltage dynamics at the same time. Instead, this time constant is a consequence of a given requisite of power sharing and operating point.

The time constant of the dynamics of frequency of NLD-AH-dVOC is zero. Therefore, we cannot design the dy-

Table 1. Configuration of the Proposed Unified GFM Control Framework for each Method. [1]

Method	τ_v	K_q	K_{vf}	τ_f	K_p	S_V	S_P
Droop	$\frac{1}{\omega_q}$	m_q	0	$\frac{1}{\omega_p}$	m_p	1	1
Sync-VSM	$\frac{K}{D_q}\frac{1}{\omega}$	$\frac{1}{D_q}$	$\frac{KD_p}{JD_q}\frac{E}{\omega^2}\left(1+\frac{1}{D_p}\frac{(\omega p^*-p\omega^*)}{\omega^*\omega(\omega^*-\omega)}\right)$	$\frac{J}{D_p}$	$\frac{1}{D_p}\frac{1}{\omega}\left(1-\frac{(\omega^*-\omega)}{\omega^*}\frac{p^*}{(p^*-p)}\right)$	1	0
NLD-AH-dVOC	$\frac{1}{\mu}\frac{1}{E(E^*+E)}$	$\frac{2\eta}{3\mu}\frac{1}{E^2(E^*+E)}$	0	0	$\frac{2\eta}{3}\frac{1}{E^2}$	0	0
LD-AH-dVOC	$\frac{1}{\sigma}\frac{1}{E}$	$\frac{2\rho}{3\sigma}$	0	0	$\frac{2\rho}{3}$	0	0

namics of this quantity. Instead, frequency changes occur instantaneously, with its value being defined by an algebraic relationship.

The voltage which is considered for regulation and the voltage which is used to calculate active and reactive powers in NLD-AH-dVOC are both the voltage of the internal model of the control model.

From the fourth line of Table 1, we can see that LD-AH-dVOC the parameters for steady-state power sharing regulation are constant, which clearly shows an enhancement as compared to NLD-AH-dVOC. The time constant of voltage dynamics is function of E and σ, therefore similarly to NLD-AH-dVOC, it is not possible to specify both steady-state power sharing and voltage dynamics at the same time. With this technique, frequency changes occur instantaneously, similarly to NLD-AH-dVOC.

In LD-AH-dVOC, the voltage which is considered for regulation and the voltage which is used to calculate active and reactive powers are both the voltage of the internal model of the control model.

4. RESULTS AND ANALYSIS

The studied GFM methods, in this work seen as instantiations of the proposed unified GFM control framework, are analyzed *in silico* concerning the steady-state droop relationships and dynamics of voltage and frequency via simulations in Matlab/Simulink™.

The steady-state droop curves, obtained by analytical solution of the steady-state droop relationships of each GFM technique, are presented with a similar appearance as those presented Johnson et al. (2022), where frequency and voltage are plotted agains active and reactive power errors.

The methods are parameterized with similar specifications, first for a operation with tight regulation of frequency and voltage, with $d_\omega^{pu} = 0.0033$ (0.33% frequency droop) and $d_v^{pu} = 0.04$ (4.0% voltage droop). The results are shown in Figure 3-(a)-(b). It can be seen that it clearly exists a strong relationship between active power p and frequency $\omega = 2\pi f$, and between reactive power q and reference voltage E.

It can be seen from these results that Droop Control, Synchronverter and LD-AH-dVOC presented similar steady-state results, which confirms that close to synchronous frequency the nonlinearities presented in Synchronverter method present small influence. On the other hand, NLD-AH-dVOC presented a more detachable influence from the nonlinearity presented in the Q/V droop relationship and the coupling between the reactive and active power loops. For this parameterization, the maximum deviations of frequency and voltage from the responses of the GFM techniques is about 25 mHz and 0.006 pu, respectively.

Subsequently, the controllers were configured for a weakly regulated operation, with $d_\omega^{pu} = 0.05$ (5.0% frequency droop) and $d_v^{pu} = 0.1$ (10.0% voltage droop). The results are shown in Figure 3-(c)-(d), where it can be observed, as expected, the P/f and Q/V droop relationships for these techniques. In contrast to the results obtained for tightly regulated operation, these presented more dissimilarities between the steady-state behavior for Synchronverter and Droop Control. This is due to the nonlinearity presented in synchronverter P/f droop relationship, as described in (17), which is more severe for weakly regulated operation. Furthermore, NLD-AH-dVOC presented a stronger influence of the nonlinearity in the Q/V droop relationship and the coupling between reactive and active power loops became more severe when compared to tightly regulated operation. For this parameterization, the maximum deviations of frequency and voltage from the responses of the GFM techniques is about 1.2 Hz and 0.03 pu, respectively.

Next we consider the characterization of the dynamics of GFM techniques of frequency and voltage. To do so, we simulate the system depicted in Figure 1 for weak regulation of voltage and frequency. From the parameterization of the AH-dVOC techniques we calculated the time constant of voltage at nominal voltage, which is approximately $15ms$, and then selected this value for the time constant of dynamics of voltage of Droop and Synchronverter. The time constant of frequency is arbitrary defined as 2 ms.

By changing the references of reactive power q^*, we induce step transients in voltage, which are shown in Figure 4. It can be seen that the calculated time constants of the AH-dVOC-based techniques are in accordance to the transients shown, which validates the proposed approach concerning the dynamics of voltage. It is interesting to note that, even though it is a variable parameter, the time constant of the Synchronverter did not presented noticeable variations for the presented transients.

We change the references of active power p^* to cause step transients in frequency, whose results are shown in Figure 5. It can be seen that the obtained transients are in

[1] See (16) for consideration on false singularities in $\omega = \omega^*$ and $p = p^*$ of parameters K_{vf} and K_p, respectively, in Synchronverter configuration.

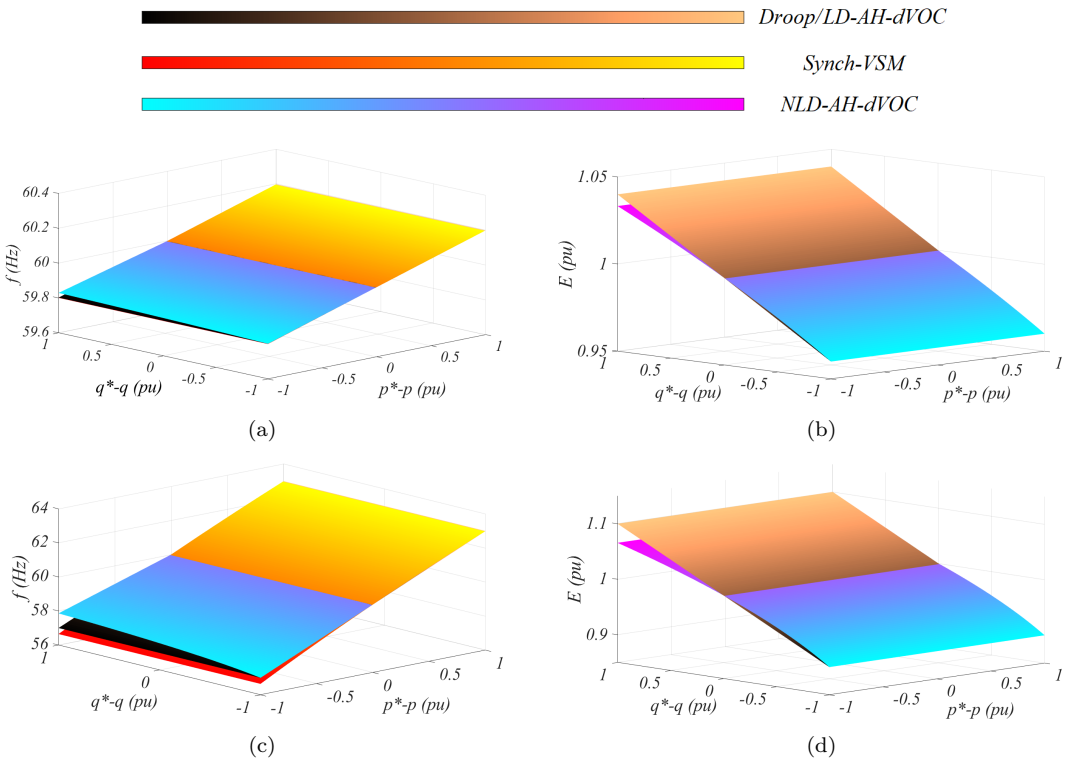

Figure 3. Numeric Analysis of the Proposed Unified GFM Control Framework Configured as Droop Control, Synchronverter and dVOC for lines dominantly inductive. Results for Tightly Regulation: (a) Frequency *vs* Active and Reactive Power Errors, (b) Voltage *vs* Active and Reactive Power Errors. Results for Weakly Regulation: (c) Frequency *vs* Active and Reactive Power Errors, (d) Voltage *vs* Active and Reactive Power Errors.

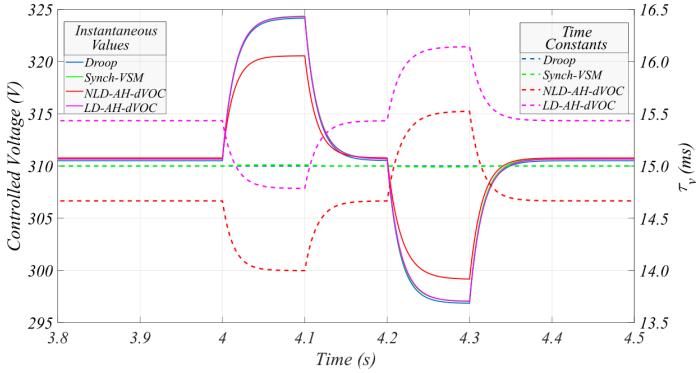

Figure 4. Dynamics of Voltage of GFM Methods for Step Transients of Reactive Power Reference.

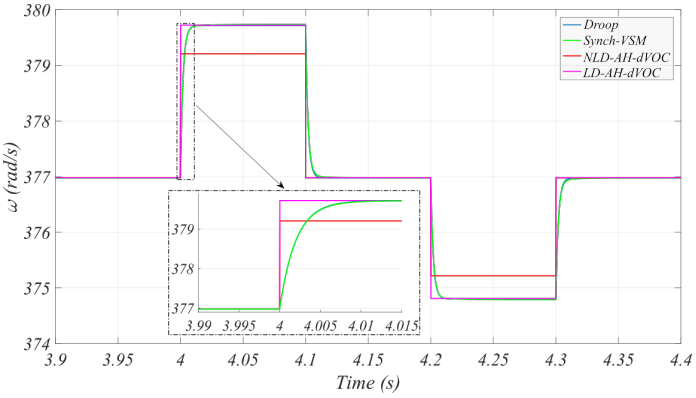

Figure 5. Dynamics of Frequency of GFM Methods for Step Transients of Active Power Reference.

accordance to the designed time constants of dynamics of frequency of the Synchronverter and Droop Control, which were set to 2 ms. For AH-dVOC techniques, the transitions in frequency are instantaneous, as predicted by their time constants of frequency in Table 1. Therefore, the dynamics of frequency of the proposed model is validated.

5. CONCLUSIONS

We proposed a unified GFM Control framework, and studied the implementation of four known GFM strategies as instantiations of the proposed model. Based on simulation results, we characterized the strategies for steady-state power sharing and dynamic responses, showing that these techniques have similarities in their actuation, where the differences, due to nonlinearities, are translated into the dependence on operating point of the parameters of the proposed model. This work brought new insights on the studied GFM techniques, developing technology-agnostic metrics with physical meaning for steady-state and dynamic behaviors for GFM methods, an important requisite for the interoperability of grid-connected inverter units. For future work, we indicate the validation of the proposed framework with experimental results.

REFERENCES

Abrantes-Ferreira, A.J.G. and Lima, A.M.N. (2021). Comparative performance analysis of grid-forming strategies applied to disconnectable microgrids. In *2021 Brazilian Power Electronics Conference (COBEP)*, 01–08. IEEE.

Akagi, H., Watanabe, E.H., and Aredes, M. (2017). *Instantaneous power theory and applications to power conditioning*. John Wiley & Sons.

Alassi, A., Ahmed, K., Egea-Alvarez, A., and Ellabban, O. (2020). Performance evaluation of four grid-forming control techniques with soft black-start capabilities. In *Conf. Rec. IEEE/ICRERA*, 221–226.

Arghir, C. and Dörfler, F. (2019). The electronic realization of synchronous machines: Model matching, angle tracking, and energy shaping techniques. *IEEE Trans. Power Electron.*, 35(4), 4398–4410.

Awal, M. and Husain, I. (2020). Unified virtual oscillator control for grid-forming and grid-following converters. *IEEE Trans. Emerg. Sel. Topics Power Electron.*

Baker, K., Bernstein, A., Dall'Anese, E., and Zhao, C. (2017). Network-cognizant voltage droop control for distribution grids. *IEEE Transactions on Power Systems*, 33(2), 2098–2108.

Bouzid, A.M., Guerrero, J.M., Cheriti, A., Bouhamida, M., Sicard, P., and Benghanem, M. (2015). A survey on control of electric power distributed generation systems for microgrid applications. *Renewable and Sustainable Energy Reviews*, 44, 751–766.

Colombino, M., Groß, D., Brouillon, J.S., and Dörfler, F. (2019). Global phase and magnitude synchronization of coupled oscillators with application to the control of grid-forming power inverters. *IEEE Trans. Autom. Control*, 64(11), 4496–4511.

D'Arco, S. and Suul, J.A. (2013). Equivalence of virtual synchronous machines and frequency-droops for converter-based microgrids. *IEEE Trans. Smart Grid*, 5(1), 394–395.

Du, W., Chen, Z., Schneider, K.P., Lasseter, R.H., Nandanoori, S.P., Tuffner, F.K., and Kundu, S. (2019). A comparative study of two widely used grid-forming droop controls on microgrid small-signal stability. *IEEE Trans. Emerg. Sel. Topics Power Electron.*, 8(2), 963–975.

Ebrahimi, M., Khajehoddin, S.A., and Karimi-Ghartemani, M. (2019). An improved damping method for virtual synchronous machines. *IEEE Trans. Sustain. Energy*, 10(3), 1491–1500.

Gomes, L.d.N., Abrantes-Ferreira, A.J.G., Dias, R.F.d.S., and Rolim, L.G.B. (2022). Synchronverter-based statcom with voltage imbalance compensation functionality. *IEEE Trans. Ind. Electron.*, 69(5), 4836–4844.

Johnson, B., Roberts, T., Ajala, O., Dominguez-Garcia, A., Dhople, S., Ramasubramanian, D., Tuohy, A., Divan, D., and Kroposki, B. (2022). A generic primary-control model for grid-forming inverters: Towards interoperable operation & control. In *Conf. Rec. HICSS*.

Johnson, B.B., Dhople, S.V., Hamadeh, A.O., and Krein, P.T. (2013). Synchronization of parallel single-phase inverters with virtual oscillator control. *IEEE Trans. Power Electron.*, 29(11), 6124–6138.

Lasseter, R.H., Chen, Z., and Pattabiraman, D. (2019). Grid-forming inverters: A critical asset for the power grid. *IEEE Trans. Emerg. Sel. Topics Power Electron.*, 8(2), 925–935.

Leonhard, W. (2001). *Control of electrical drives*. Springer Science & Business Media.

Lin, Y., Eto, J., Johnson, B., Flicker, J., Lasseter, R., Pico, H.V., Seo, G.S., Pierre, B., Ellis, A., Miller, J., and Yuan, G. (2022). Pathways to the next-generation power system with inverter-based resources: Challenges and recommendations. *IEEE Electrification Magazine*, 10(1), 10–21.

Lu, M., Dutta, S., Purba, V., Dhople, S., and Johnson, B. (2019). A grid-compatible virtual oscillator controller: Analysis and design. In *Conf. Rec. IEEE/ECCE*, 2643–2649. IEEE, Baltimore, MD, USA.

Matevosyan, J., MacDowell, J., Miller, N., Badrzadeh, B., Ramasubramanian, D., Isaacs, A., Quint, R., Quitmann, E., Pfeiffer, R., Urdal, H., et al. (2021). A future with inverter-based resources: Finding strength from traditional weakness. *IEEE Power and Energy Magazine*, 19(6), 18–28.

Meng, X., Liu, J., and Liu, Z. (2018). A generalized droop control for grid-supporting inverter based on comparison between traditional droop control and virtual synchronous generator control. *IEEE Trans. Power Electron.*, 34(6), 5416–5438.

Milano, F., Dörfler, F., Hug, G., Hill, D.J., and Verbič, G. (2018). Foundations and challenges of low-inertia systems. In *Conf. Rec. IEEE/PSCC*, 1–25. IEEE, Dublin, Ireland.

O'Malley, M., Bowen, T., Bialek, J., Braun, M., Cutululis, N., Green, T., Hansen, A., Kennedy, E., Kiviluoma, J., Leslie, J., Li, Y., Matevosyan, J., McDowell, J., Miller, N., Pettingill, P., Ramasubramanian, D., Robinson, L., Schaefer, C., and Ward, J. (2021). Enabling power system transformation globally: A system operator research agenda for bulk power system issues. *IEEE Power and Energy Magazine*, 19(6), 45–55.

O'Rourke, C.J., Qasim, M.M., Overlin, M.R., and Kirtley, J.L. (2019). A geometric interpretation of reference frames and transformations: dq0, clarke, and park. *IEEE Trans. Energy Convers.*, 34(4), 2070–2083. doi: 10.1109/TEC.2019.2941175.

Rosso, R., Wang, X., Liserre, M., Lu, X., and Engelken, S. (2021). Grid-forming converters: control approaches, grid-synchronization, and future trends-a review. *IEEE Open Journal of Industry Applications*.

Sinha, M., Dörfler, F., Johnson, B.B., and Dhople, S.V. (2015). Uncovering droop control laws embedded within the nonlinear dynamics of van der pol oscillators. *IEEE Control Netw. Syst.*, 4(2), 347–358.

Smith, J.C. and Lew, D. (2021). Variable renewable energy: The way of the future [guest editorial]. *IEEE Power and Energy Magazine*, 19(6), 14–16.

Sun, Y., Hou, X., Yang, J., Han, H., Su, M., and Guerrero, J.M. (2017). New perspectives on droop control in ac microgrid. *IEEE Trans. Ind. Electron.*, 64(7), 5741–5745.

Tôrres, L.A., Hespanha, J.P., and Moehlis, J. (2015). Synchronization of identical oscillators coupled through a symmetric network with dynamics: A constructive approach with applications to parallel operation of inverters. *IEEE Trans. Autom. Control*, 60(12), 3226–3241.

Wu, H. and Wang, X. (2018). Design-oriented transient stability analysis of grid-connected converters with power synchronization control. *IEEE Trans. Ind. Electron.*, 66(8), 6473–6482.